analytical chemistry

pubs.acs.org/ac Article

Rational Control of Interfacial Spontaneous Redox Reactions by Modulating Single-Microdroplet Charging

Xiangyu Wang,[#] Jin Han,[#] Xin Diao, Xiaofei Wang, Chen Zeng, Yongyi Li, Jianing Wang,* Zongwei Cai, and Zhenwei Wei*

Cite This: *Anal. Chem.* 2026, 98, 850−859 Read Online

ACCESS | Metrics & More | Article Recommendations | Supporting Information

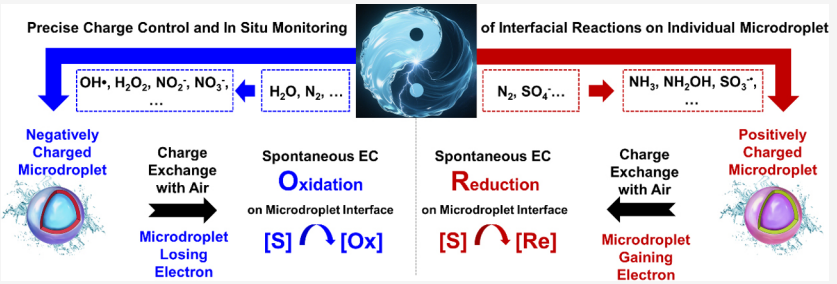

ABSTRACT: Microdroplet chemistry has garnered increasing attention due to the discovery that extreme redox reactions can spontaneously occur at droplet interfaces. Most current studies rely on ensemble-averaged aerosol behavior, yet each microdroplet may exhibit vastly different reactivities depending on its size and charge polarity. To address this problem, we developed a dielectric barrier electrospray platform, which treats the entire liquid volume confined within the emitter tip as a single stationary microdroplet reactor. This setup enables precise charge control and in situ monitoring of interfacial reactions in this isolated, picoliter-to-nanoliter droplet. Our results reveal that redox processes at microdroplet interfaces can proceed as spontaneous interfacial electrochemical reactions, driven by the polarity of microdroplet charge. The reaction mechanism can be explained well by a modified microdroplet electric double-layer model. The reaction Faradaic current was measured at 58 pA, corresponding to a current density of 1.7 mA/m^2—remarkably consistent with estimations of charged microdroplet activity in atmospheric clouds. With this platform, we demonstrated that the disproportionation of nitrogen at microdroplet interfaces originates from the reaction polarity being defined at the single-droplet level by its charge, each selectively catalyzing the oxidation or reduction of N_2. These findings not only shed light on the atmospheric nitrogen cycle but also offer critical theoretical guidance for future bulk nitrogen chemistry enabled by microdroplet catalysis.

INTRODUCTION

In 2011, the phenomenon of accelerated chemical reactions at microdroplet interfaces was first discovered using electrospray ionization mass spectrometry,[1−3] sparking widespread interest in microdroplet chemistry. As research progressed, it was further revealed that microdroplet interfaces exhibit unique redox properties, enabling the catalysis or spontaneous occurrence of redox reactions that are otherwise challenging in bulk solutions.[4−10] For instance, hydroxyl radicals were found to spontaneously form on the surfaces of water microdroplets,[11−13] triggering a series of oxidation reactions, including the Dakin reaction,[12] Baeyer−Villiger oxidation,[14] C−H oxidation,[15] and C−N coupling reactions.[16,17] Additionally, microdroplet interfaces can undergo reduction reactions by gaining electrons,[18] as in the spontaneous reduction of metal ions to form clusters or nanoparticles[19,20] and the generation of highly reactive radical anions.[21−23] Despite these advances, the driving forces and polarity control of redox reactions at microdroplet interfaces remain a widely debated, yet unresolved, scientific challenge.

A prevailing hypothesis attributes these phenomena to the ultrahigh electric fields at microdroplet interfaces, fields that reach magnitudes of 10^9 V/m.[2,24−27] This hypothesis is supported by calculations[28] and Raman spectroscopy measurements.[24,29] Although the ultrahigh electric field hypothesis provides a thermodynamic rationale for the occurrence of extreme redox reactions, it struggles to explain the dual redox behavior of microdroplets—why they sometimes exhibit oxidative properties and other times reductive properties.[28,30,31] Notably, although most microdroplet chemistry

Received: September 28, 2025
Revised: November 20, 2025
Accepted: December 10, 2025
Published: December 20, 2025

https://doi.org/10.1021/acs.analchem.5c06042
Anal. Chem. 2026, 98, 850−859

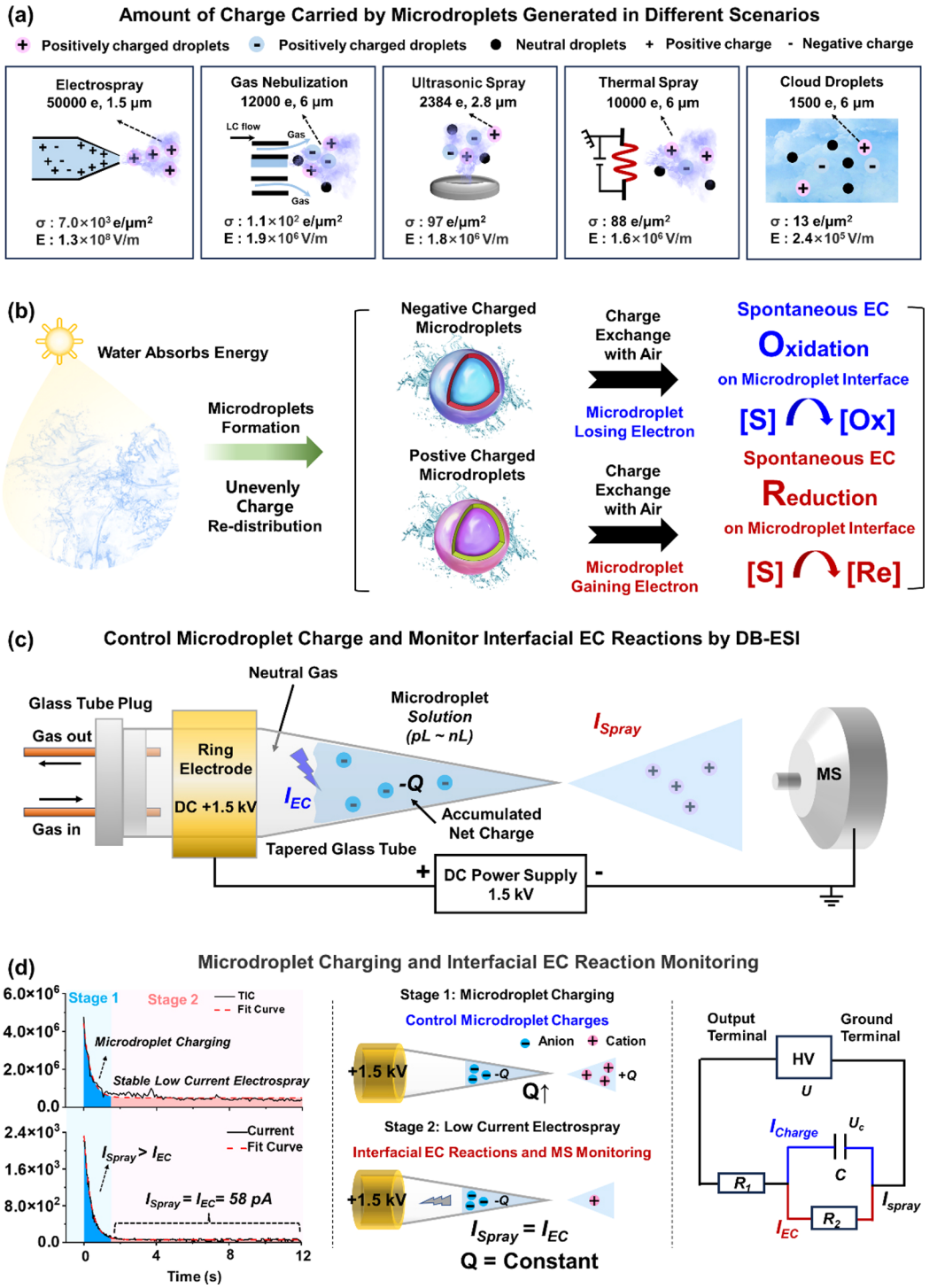

Figure 1. Mass spectrometric monitoring of interfacial EC reactions of specific microdroplets with controlled charge and polarity. (a) The size and charge of microdroplets reported in the literature for electrospray,[35,36] ultrasonic spray,[33,38] pneumatic spray,[13,37] thermal spray,[35,39] and cloud droplets.[40] The surface charge density (σ) and charge-induced electric field strength (E) for each type of microdroplet are calculated and displayed. (b) Charge distribution and redox reactions in natural aerosols. When microdroplets in aerosols undergo random splitting, the charge distribution becomes uneven, resulting in some microdroplets carrying negative charges and some positive charges. Positively charged microdroplets likely undergo reduction reactions at the gas−liquid interface, while negatively charged microdroplets undergo oxidation reactions. (c) Setup of the DB-ESI system. (d) The mechanism of DB-ESI to control charges as well as analysis of interfacial EC reactions of a specific microdroplet. The charge of the microdroplet is determined by capacitor charging (Stage 1), and low-current electrospray (Stage 2) is used for continuous interfacial EC reaction monitoring.

experiments generate neutral microdroplet aerosols through methods such as ultrasonic spraying, this does not imply that every microdroplet is electrically neutral.[32−34] Historical studies on the charge distribution of aerosol microdroplets have consistently shown that both positively and negatively charged microdroplets coexist in aerosols generated by

https://doi.org/10.1021/acs.analchem.5c06042
Anal. Chem. 2026, 98, 850−859

electrospray,[35,36] pneumatic spray,[13,37] ultrasonic spray,[33,38] and thermal spray,[35,39] as well as in naturally formed aerosols such as clouds and fogs[40−43] (Figure 1a). Therefore, the reaction property of a specific microdroplet vs ensembles of microdroplets can be totally different. A possible hypothesis (Figure 1b) is that the redox reactivity of a specific microdroplet is intrinsically determined by the microdroplet's polarity, representing a fundamental electrochemical process occurring at gas−liquid interfaces. As microdroplet aerosols contain both positive and negative droplets, they may simultaneously exhibit both oxidative and reductive reactivity measured at the macroscopic scale, as reported in recent studies.[28,30] However, validating this idea involves a bottleneck problem in the microdroplet research field: how to precisely control the charge polarity of a single droplet and accurately monitor the reactions occurring at its gas−liquid interface.

EXPERIMENTAL SECTION

Chemicals and Materials

Melatonin (98%), reserpine (98%), threonic acid (98%), angiotensin II (90%), and ammonium bicarbonate (NH_4HCO_3, 99.9%) were bought from Shanghai Macklin Biochemical Co., Ltd. (Shanghai, China). Sennoside B (purity: analytical reference), adenosine diphosphate (ADP, 98%), *o*-phenylenediamine (OPD, 98%), cobalt(II) sulfate heptahydrate ($CoSO_4{\cdot}7H_2O$, 99.99%), deuterium water (99.9%), and insulin (27 U/mg) were obtained from Meryer Chemical Technology Co., Ltd. (Shanghai, China). Caffeine (98%) was purchased from Shanghai Reagent Factory No. 2 (Shanghai, China). 3-Aminobenzeneboronic acid (3-ABBA, 98%)was bought from Bidiphar (Shanghai, China). Formic acid (FA, LC−MS grade) was obtained from TCI Chemicals (Shanghai, China). Trimethylaminomethane (Tris, AR), ethylenediamine tetraacetic acid disodium salt (EDTA, AR), ammonium acetate (NH_4Ac, AR), hydrogen peroxide (H_2O_2, AR), magnesium chloride ($MgCl_2$, AR), and manganese chloride ($MnCl_2$, AR) were purchased from Sinopharm Chemical Reagent Co., Ltd. (Shanghai, China). The Tris buffer solution was 50 nM Tris, 2 nM EDTA, 1 nM $MgCl_2$, and 1 nM $MnCl_2$. Borosilicate glass capillary (I.D. = 0.86 mm, O.D. = 1.5 mm, without filament) was obtained from Sutter Instrument Company (Novato, CA, USA). Purified water used in this experiment was purchased from Hangzhou Wahaha Group Co., Ltd. Nitrogen was provided by a QPNM-35H nitrogen generator (Shanghai Quan Pu Scientific Instruments Co., Ltd., Shanghai, China).

Fabrication of Electrospray Ionization Source Emitters

Borosilicate glass capillaries were pulled by a Sutter Instrument CO. P-97 puller (Novato, CA, USA) and manually cut to make the electrospray emitters with an I.D. of 18 to 22 μm (observed by a microscope, YXL3230, Beijing Dayueweijia Technology Co., Ltd., Beijing, China). The parameters of P-97 were as follows: HEAT = 575, PRESSURE = 200, VELOCITY = 150, TIME = 0, and PULL = 0. Borosilicate glass capillaries were pulled by a Sutter Instrument Co. P-97 puller (Novato, CA, USA) to make the electrospray (ESI) emitters with an I.D. of 1.0 to 2.5 μm (observed by a microscope, YXL3230, Beijing Dayueweijia Technology Co., Ltd., Beijing, China). The parameters of P-97 were as follows: HEAT = 574, PRESSURE = 600, VELOCITY = 15, DELAY = 250, and PULL = 0.

Sampling Method

In the experiment, capillary force was utilized for sampling microdroplet solution into the emitter with the sampling volume controlled by adjusting the immersion time of the emitter tip in the sample solution. When the immersion duration ranged from 10 to 12 s, the collected sample volume was measured between 9.6 and 10.3 nL. An immersion time of approximately 0.4 s yielded a sampling quantity of about 10 pL (Figure S1).

Dielectric Barrier Electrospray Ionization (DB-ESI) System

The ring electrode was a stainless steel hollow cylinder with an I.D. of 1.6 mm, an O.D. of 1 cm, and a length of 1 cm, which was mounted on an electrically insulated 3D moving stage (x, y, z). A tapered nESI emitter was placed passing through the hollow ring electrode. The emitter tip O.D. was measured at 1.5−2.0 μm. A DC voltage (+1.5 or −1.2 kV) was applied to the electrode to generate an electrostatic field. The electrode-to-solution distance (distance between the electrode front cross-section and the solution rear interface) was typically maintained at 9−12 mm. The distance between the emitter tip and the MS inlet (usually 5 mm) was adjustable via the 3D moving stage (Figure 1c).

Measurement of Electrospray Current

The electrospray current measurement experiment was carried out in a Faraday cage (Figure S2). The Faraday cage was made of a 99.9% pure copper mesh (200 mesh). The Faraday cup used to receive the ion current was made of stainless steel. The ammeter was a KEYSIGHT B2981B femtoammeter/picoammeter (Keysight Technologies, Santa Rosa, California, USA). When testing the current, the Faraday cage, ammeter, and high-voltage power supply were all well grounded, and there was no electromagnetic interference or large instrument operation nearby.

RESULTS AND DISCUSSION

Precise Charge Control and Continuous Interfacial Reaction Monitoring of Specific Microdroplets

In this work, we address this challenge by developing dielectric barrier electrospray ionization mass spectrometry (DB-ESI-MS). This approach enables stable maintenance and precise net charge control for a specific microdroplet with the minimum size reaching 10 pL (equivalent to a 13 μm spherical droplet) while simultaneously allowing ultrasensitive and continuous in situ reaction monitoring of microdroplet interfacial electrochemistry by high-resolution mass spectrometry (HRMS). The DB-ESI system consists of three main components: a tapered capillary, a ring electrode, and a high-voltage DC power supply (Figure 1c). The tapered glass capillary utilizes capillary force to control the siphoning of pL-to-nL volumes of microdroplet solutions (Figure S1). As illustrated in Figure 1c, when a DC high voltage is applied to the ring electrode, the resulting electrostatic field induces polarization of the microdroplet, leading to electrospray at the emitter tip and generating a spray current (I_{spray}). This electrospray not only causes the separation of positive and negative charges within the microdroplet, gradually charging it, but also carries substances from the microdroplet to MS for analysis. Notably, I_{spray} comprises two components: the capacitive charging current (I_{charge}, non-Faradaic current) due to microdroplet polarization and the interfacial EC reaction current (I_{EC}, Faradaic current) at the gas−liquid interface. The

https://doi.org/10.1021/acs.analchem.5c06042
Anal. Chem. 2026, 98, 850−859

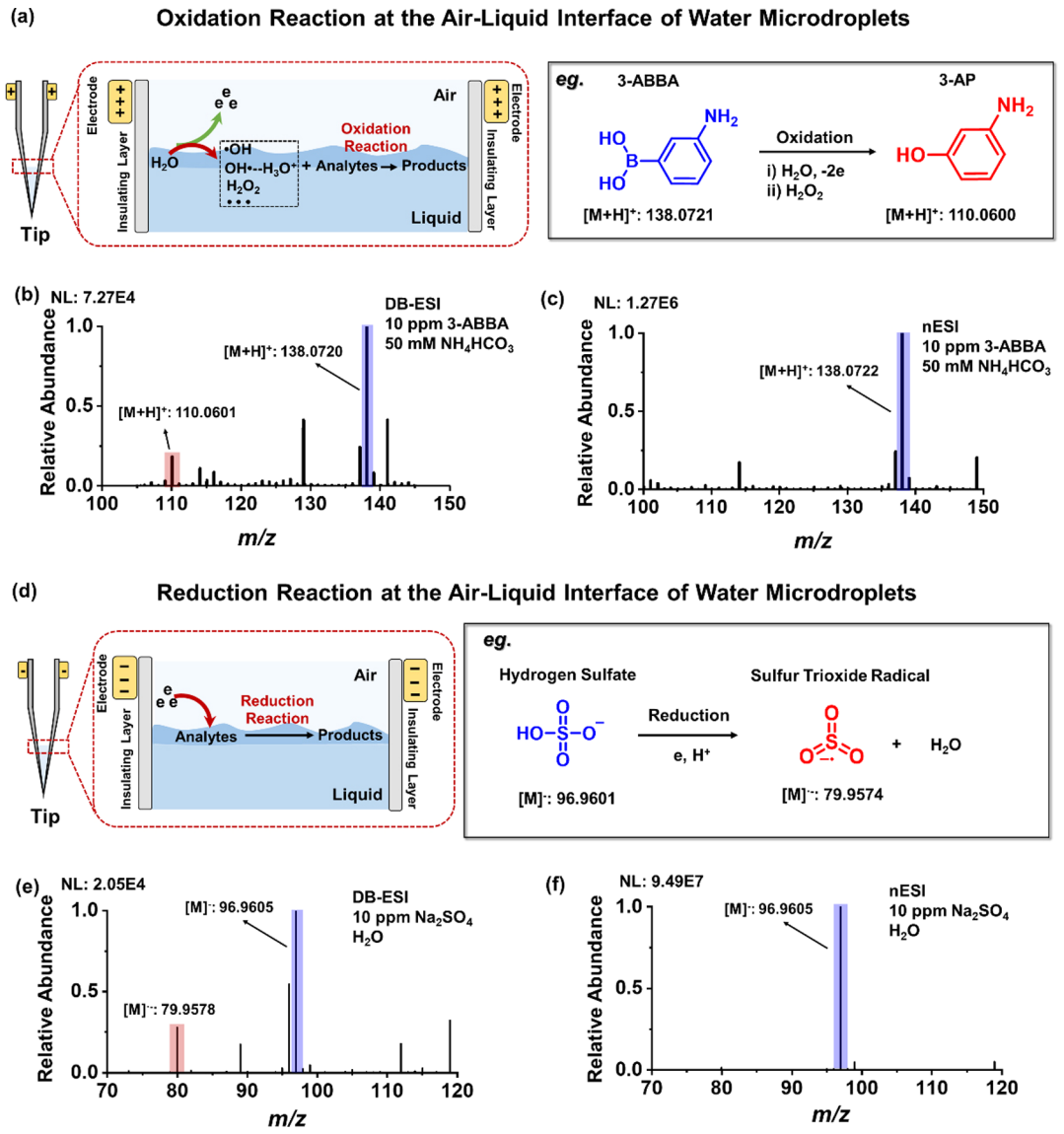

Figure 2. EC redox reactions at the gas−liquid interface of water microdroplets. (a) Evidence of oxidation reactions at negatively charged interfaces. The process can be probed by the oxidation reaction of 3-ABBA to 3-AP. (b) The mass spectrum of DB-ESI analysis of a solution containing 100 ppm 3-ABBA and 50 mM NH_4HCO_3. The 3-ABBA ($[M + H]^+$, m/z 138.0720) was observed to oxidize to 3-AP ($[M + H]^+$, m/z 110.0601), indicating the formation of hydroxy radicals and peroxides at the interface. (c) Control experiment using nESI: no oxidation product was observed in bulk conditions. (d) Evidence of reduction reactions at positively charged interfaces: hydrogen sulfate ions were reduced to sulfite radical anions. (e) The mass spectrum of DB-ESI of a 10 ppm sodium sulfate aqueous solution. Reduction of HSO_4^- ($[M]^-$, m/z 96.9605) to $SO_3^{-\bullet}$ ($[M]^{-\bullet}$, m/z 79.9578) was observed. (f) Control experiment using nESI: no reduction product was observed in bulk conditions.

presence of I_{EC} explains why DB-ESI can hold continuous electrospray for a very long time, which is quite different from previously reported induced ESI methods.[44,45] In conventional ESI, EC reactions at the electrode-solution interfaces are well-established;[46−48] however, DB-ESI physically isolates the electrode from solution, preventing direct charge and compound exchange. Therefore, the faradaic current (I_{EC}) and the corresponding redox products in DB-ESI can arise solely from EC reactions between a charged microdroplet and surrounding air.

Figure 1D demonstrates the behavior of a 10 nL glutathione (GSH, 10 ppm) aqueous solution under a +1.5 kV electrode voltage. Both the total ion chronogram (TIC) from mass spectrometry and direct measurements of I_{spray} (see Figure S2 for the setup used to measure weak electrospray currents) reveal that the microdroplet underwent a rapid charging process within 1.5 s due to the electrostatic field, followed by a stable spray process lasting several hours (Figure S3, mass spectra of continuous stable spray over hours). During the charging stage (Stage 1), the microdroplet in the emitter accumulated negative charge due to positive spray, which gradually weakened the electric field at the emitter tip, causing I_{charge} to decrease over time. As the charge on the microdroplet increased, the interfacial reaction current (I_{EC}) at the gas−liquid interface also rose. Although I_{EC} may initially be much smaller than I_{charge}, it becomes the dominant contributor to I_{spray} during the stable spray stage (stage 2), which can last for hours. The equivalent circuit of DB-ESI is a series−parallel RC circuit (Figure 1d), where the solved expressions of I_{charge}, I_{EC}, and I_{spray} are as follows (detailed solution shown in additional discussion in Supporting Information, Section 2):

https://doi.org/10.1021/acs.analchem.5c06042
Anal. Chem. 2026, 98, 850−859

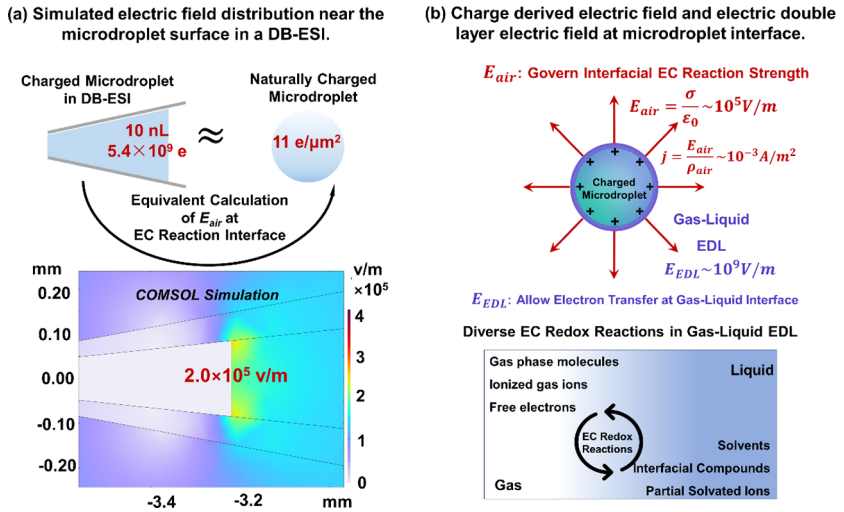

Figure 3. Modified microdroplet electric double layer model to account for the observed interfacial electrochemistry. (a) A COMSOL simulation was performed on a 10 nL solution carrying a charge of 8.7×10^{-10} C (5.4×10^9 e). The simulated E_{air} near the droplet surface in DB-ESI was found to be 2.0×10^5 V/m, which corresponds to the E_{air} value of a spherical droplet with a charge density of 11 e/μm^2. (b) Charge-derived electric field (E_{air}) and electric double layer electric field (E_{EDL}) at the microdroplet interface. The EDL between a charged microdroplet and the surrounding gas generates an extremely high internal electric field. E_{air}, denoting the electric field strength penetrating into the gaseous side of this layer, directly dictates the rate or current of electrochemical reactions on the microdroplet surface.

$$I_{charge}(t) = \frac{dQ}{dt} = \frac{U}{R_1} e^{-(R_1+R_2)/R_1R_2Ct} \quad (1)$$

$$I_{EC}(t) = \frac{Q}{CR_2} = \frac{U}{R_1+R_2}(1 - e^{-(R_1+R_2)/R_1R_2Ct}) \quad (2)$$

$$I_{spray}(t) = I_{charge}(t) + I_{EC}(t) = \left(\frac{U}{R_1} - \frac{U}{R_1+R_2}\right) e^{-(R_1+R_2)/R_1R_2Ct} + \frac{U}{R_1+R_2} \quad (3)$$

By fitting the spray current versus time data in Figure 1d using eq 3, the following results are obtained:

$$I_{spray}(\text{pA}) = 2280 \times \exp\left(-\frac{t}{0.37}\right) + 58 \quad (R^2 = 0.9938) \quad (4)$$

$$I_{charge}(\text{pA}) = 2338 \times \exp\left(-\frac{t}{0.37}\right) \quad (5)$$

Based on the fitting results from eq 4, the Faradaic current on the microdroplet interface I_{EC} in DB-ESI is 58 pA. By integrating I_{charge} (eq 5), the total charge of the 10 nL microdroplet during stable spraying was calculated to be 8.7×10^{-10} C (5.4×10^9 e). These experimental results demonstrate that DB-ESI enables precise control over the charge polarity and magnitude of a specific microdroplet while also providing stable, long-lasting electrospray for reaction monitoring of the microdroplet. We further evaluated the analytical performance of DB-ESI with several typical analytes (Table S1), demonstrating that DB-ESI had ultrahigh sensitivity with a LOD of attogram (ag) level (additional discussion in Supporting Information, Section 3, Figures S4–S6). This exceptional sensitivity makes DB-ESI highly suitable for real-time in situ monitoring of EC reactions at microdroplet interfaces.

Interfacial EC Reaction Governed by Microdroplet Charge and Polarity

Using the DB-ESI system, we validated the hypothesis that redox reactions occurring at microdroplet interfaces are fundamentally governed by the charge polarity of the microdroplets through EC mechanisms. In these experiments, we used a 10 pL microdroplet volume (equivalent to a 13 μm spherical droplet) for analysis. First, we demonstrated that negatively charged water microdroplets are more prone to oxidation reactions in air. Aminophenylboronic acid (3-ABBA, 10 ppm) was employed as probe molecules[13,49−51] to capture $^{\bullet}$OH or H_2O_2 to produce 3-aminophenol (3-AP) during DB-ESI analysis of 10 pL water microdroplets (Figures 2a and S7). The DB-ESI-MS results confirmed the gradual oxidation of 3-ABBA ($[M + H]^+$, m/z 138.0720) to 3-AP ($[M + H]^+$, m/z 110.0601) at the microdroplet interface (Figures 2b, S8, and S9), proving that the spontaneous EC reaction on negative microdroplet interfaces generated oxidizing reagents such as $^{\bullet}$OH and H_2O_2, which triggered a variety of oxidation reactions within the microdroplets.[14,52] In contrast, control experiments using nESI to directly analyze 3-ABBA bulk solutions did not observe the oxidation of 3-ABBA to 3-AP (Figures 2C and S9).

To demonstrate that positively charged microdroplet interfaces are more likely to undergo reduction reactions, we selected the reduction of sulfate to the sulfite radical anion ($SO_3^{-\bullet}$) as a model reaction (Figure 2d). For 10 pL of Na_2SO_4 aqueous microdroplets (10 ppm), DB-ESI simultaneously detected HSO_4^- ($[M]^-$, m/z 96.9605) and $SO_3^{-\bullet}$ ($[M]^{-\bullet}$, m/z 79.9578) (Figure 2e). The ratio of the reduction product $SO_3^{-\bullet}$ to the reactant HSO_4^- increased over time, indicating the accumulation of the EC reaction product (Figure S10). In contrast, no reduction reaction was observed in the nESI control experiments (Figure 2f).

By comparing the kinetics of oxidation and reduction reactions at the microdroplet interface (Figures S9b and S10b), we found that oxidation reactions proceed more rapidly. This is likely because water itself can participate in

https://doi.org/10.1021/acs.analchem.5c06042
Anal. Chem. 2026, 98, 850−859

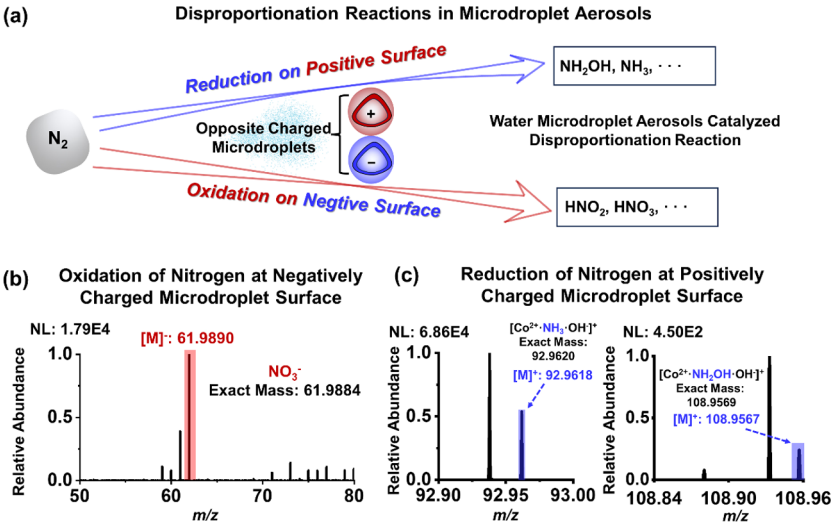

Figure 4. Microdroplet-catalyzed N_2 disproportionation reaction. The microdroplet volume used in these experiments was 10 nL. (a) N_2 underwent a disproportionation reaction in the microdroplets. The microdroplets with positive charges on the surface underwent a reduction reaction, generating a series of reduction products such as ammonia and hydroxylamine. The microdroplets with negative charges on the surface underwent an oxidation reaction, generating a series of oxidation products such as nitric acid and nitrous acid. (b) HRMS spectra of nitrate ions (NO_3^-, m/z, 61.9890) generated on the negatively charged microdroplet interface. (c) HRMS spectra of $[Co^{2+}{\cdot}NH_3{\cdot}HO^-]^+$ (m/z, 92.9619) and $[Co^{2+}{\cdot}NH_2OH{\cdot}HO^-]^+$ (m/z, 108.9569) generated at the interface of positively charged microdroplets.

oxidation reactions at the interface, forming reactive species such as $^{\bullet}OH/(H_2O)_2^{+\bullet}$[53,54], which further react with substrates in the microdroplet. In contrast, the reduction of water at the interface generates active $^{\bullet}H$ species, or electrons rapidly diffuse. As a result, reduction reactions may require direct participation of substrates at the microdroplet interface for electron transfer, leading to slower kinetics compared with oxidation processes.

Modified Microdroplet Electric Double Layer Model to Account for the Observed Interfacial Electrochemistry

Furthermore, we also explored whether the EC reactions observed on the surfaces of charged microdroplets in DB-ESI can represent spontaneous electrochemical reactions on the surfaces of naturally formed microdroplets. Figure 1a shows the charge density and the charge-induced electric field strength (E_{air}, near the microdroplet surface in the gas phase) of microdroplets generated in different ways, among which charged microdroplets in clouds showed an average diameter of 6 μm and a charge of 1500 e,[40] corresponding to a E_{air} of approximately 2.4 × 10^5 V/m and a surface charge density of 13 e/μm^2. Based on the fitting results in Figure 1d, we determined that the 10 nL solution carried a charge of 8.7 × 10^{-10} C (5.4 × 10^9 e) during stabilized DB-ESI spraying. Based on the microdroplet geometry in Figure S1, we used COMSOL simulation (Figure S11) to obtain the E_{air} of 2.0 × 10^5 V/m near the microdroplet surface in DB-ESI (Figure 3a), corresponding to the E_{air} value of a ball-shaped microdroplet with 11 e/μm^2 charge density. The above results indicate that the electrochemical processes occurring on natural microdroplet surfaces may be similar to or even stronger than those observed in DB-ESI. We calculated a Faradaic current density of 1.7 × 10^{-3} A/m^2 in DB-ESI (details in Supporting Information, Section 4). Although this current density is 1000 to 10,000 times lower than that of conventional solid–liquid electrochemical systems, the vast total surface area of microdroplets in clouds may reach a substantial magnitude, rendering microdroplet electrochemistry non-negligible in atmospheric chemical processes (a quantitative assessment of its influence is provided in Supporting Information, Section 5).

It should be clarified that E_{air} is fundamentally distinct from the interfacial electric fields with 10^8–10^{10} V/m strength at microdroplet boundaries in prior reports.[24,55,56] As these reported 10^9 V/m interfacial fields are highly consistent with the characteristic electric double layer (EDL) fields (10^8–10^{10} V/m) observed at solid–liquid EC interfaces,[57−59] hypotheses regarding the EDL at microdroplet interfaces were proposed in several recent studies.[29,60−63] For instance, Chamberlayne and Zare suggested that ion adsorption at the liquid surface constituted the primary source of EDL;[25,26] Kumar and Francisco proposed that ion pairs form a subsurface enrichment layer in microdroplets, with a superjacent ion-depleted water layer, creating interfacial electric fields significantly stronger than predicted by classical EDL models;[63] Cooks and Amotz proposed the microdroplet EDL might involve water radical cation/anion pairs;[53,54,64] Bonn et al. further elucidated the EDL dynamics at the air–aqueous electrolyte solution interface driven by ion conduction using nonlinear time-resolved vibrational sum-frequency generation.[65] The proposed EDL model at the gas–liquid interface of microdroplets provides a compelling explanation for the ultrahigh electric fields generated by molecular dissociation and ion adsorption. However, whether electrochemical reactions occur at the EDL remains unresolved due to the lack of direct and reliable experimental evidence.

As we clearly observed EC reactions and measured the Faradaic current at the gas–liquid interface, it strongly implies the EDL (E_{EDL} ca. 10^9 V/m) should also include a gas–liquid transitional region extending beyond the liquid phase of the microdroplet (Figure 3b), including solvents, interfacial compounds, and partially solvated ions in the liquid phase, as well as gas-phase molecules, ionized gas ions, and free electrons in the gas phase. The rationale of the hypothesis is from the gas breakdown theory that fields reaching 10^6 V/m can induce gas ionization,[66,67] while the E_{EDL} was three orders of magnitude exceeding this limit. Therefore, we propose a

https://doi.org/10.1021/acs.analchem.5c06042
Anal. Chem. 2026, 98, 850−859

modified microdroplet EDL model to account for the observed interfacial electrochemistry (Figure 3b): (1) the EDL-like structures formed between the charged microdroplet and surrounding gas, with ultrahigh inner electric fields (E_{EDL} ca. 10^9 V/m), may ionize surrounding gas[68−70] to generate free electrons and allow electron transfer in EDL; (2) E_{air} represents the electric field strength in the gas phase penetrating through the EDL, primarily governed by the microdroplet's surface charge density according to Coulomb's law. Its magnitude directly determines the strength/current of the microdroplet surface EC reactions.

Nitrogen Disproportionation at the Gas−Liquid Interface of a Single Microdroplet

In our recent study, we have demonstrated through scaled-up microdroplet experiments that neutral microdroplet aerosols can catalyze the disproportionation of N_2.[71] This raised a puzzling question: under identical conditions, why does the microdroplet interface simultaneously catalyze both the oxidation and reduction reactions of N_2? In the following experiments, we definitively demonstrate that N_2 undergoes either oxidation or reduction exclusively on microdroplet surfaces with different charge polarities (Figure 4a). We continuously introduced N_2 into deionized water to obtain a saturated N_2 aqueous solution in ambient condition (N_2 concentration ca. 25 ppm). As shown in Figure 4b, we kept the negatively charged microdroplet in the air for 1 min and clearly detected nitrate ions (NO_3^-, m/z 61.9890) in the following MS analysis. Since the HRMS experiment cannot be conducted for species of m/z lower than 50, in order to achieve HRMS of small m/z ions such as nitrite (NO_2^-), we added 28 ppm of cobalt sulfate ($CoSO_4$) to the microdroplet solution for DB-ESI analysis (Figure S12). As shown in Figure S12b,c, we observed the generation of cobalt-nitrate ($[Co^{2+}\cdot H_2O\cdot NO_3^-]^+$, m/z 138.9310) as well as cobalt-nitrite ($[Co^{2+}\cdot H_2O\cdot NO_2^-]^+$, m/z 122.9361), indicating that N_2 underwent an oxidation reaction at the negatively charged microdroplet surface to generate nitrite and nitrate. Similarly, for the positively charged microdroplet (Figure 4c), we observed the complexes of cobalt ions with NH_3 and NH_2OH, $[Co^{2+}\cdot NH_3\cdot HO^-]^+$ (m/z, 92.9619) and $[Co^{2+}\cdot NH_2OH\cdot HO^-]^+$ (m/z, 108.9569), indicating that N_2 underwent a reduction reaction at the positively charged microdroplet surface. These experiments provide clear evidence that the polarity of spontaneous EC reactions of N_2 on the microdroplet surface is governed by microdroplet charge and explains why N_2 will present a disproportionation phenomenon in aerosols. These experiments also solved a long-standing problem in the field of microdroplet research, that is, why neutral aerosols generated by pneumatic spray or ultrasonic spray sometimes behave strongly reducing, such as the spontaneous reduction of metal ions to form clusters or nanoparticles,[19,20,72] and sometimes behave oxidizing, forming hydroxyl radicals.[11−13,73]

Reactions in Charged and "Uncharged" Microdroplets

Finally, we discuss how our results relate to recent observations in "uncharged" microdroplets (probably better phrased as "ultraweakly charged microdroplets"). Since microdroplet chemistry was originally discovered in electrospray,[3] there has been a long-standing debate over whether microdroplet reactivity arises primarily from electric charge or from intrinsic interfacial properties. In our view, these two perspectives are not mutually exclusive. For example, Zhang et al. recently generated microdroplets via CO_2 dry ice bubbling in aqueous solution.[34] Charge-deflection measurements[33] showed that these droplets carry essentially no net charge, yet they still promote reactions such as Schiff-base formation and Michael addition—clear evidence of intrinsic microdroplet reactivity. However, reactions involving the generation of water radical cations or other highly reactive radical oxidants/reductants are difficult to sustain in such nearly uncharged droplets.[34] In contrast, these "extreme" redox processes occur readily in the charged microdroplets studied here. The reason, we believe, is that the droplet-borne charge itself effectively acts as a continuously supplied oxidizing or reducing driving force. For microdroplet reactions that require such extreme redox conditions, the ability to rationally modulate droplet charge is essential for achieving controlled reactivity.

CONCLUSION

In this work, we sought to uncover the fundamental factors that drive redox reactions at the interfaces of microdroplets. Previous microdroplet reaction studies have typically relied on ensemble-averaged results from aerosolized droplets, overlooking the heterogeneity of microdroplets in charge polarity, charge quantity, and droplet size—factors that can profoundly influence microdroplet interfacial chemistry. By developing a DB-ESI platform, we achieved, for the first time, long-term continuous monitoring of single microdroplets (pL-nL scale) with precisely controlled size, charge polarity, and charge quantity. Our results demonstrate a direct correlation between the droplet's electrical properties and its interfacial redox behavior, and we interpret these findings within an electrochemical framework. Through simulations and calculations, we further show that DB-ESI experiments can model the intensity of electrochemical reactions at charged microdroplet−air interfaces in nature. Notably, we report the first quantitative measurement of the interfacial electrochemical current density between microdroplets and air (1.7 mA/m^2), providing critical experimental benchmarks for understanding such processes in natural environments. We postulate that this work not only advances the mechanistic understanding of microdroplet chemistry but also establishes an experimental methodology for designing more precise and reliable microdroplet-based studies in the future.

ASSOCIATED CONTENT

Supporting Information

The Supporting Information is available free of charge at https://pubs.acs.org/doi/10.1021/acs.analchem.5c06042.

Fabrication and characterization of the DB-ESI platform; derivation of the equivalent circuit model; analytical performance and sensitivity data; kinetic profiles of interfacial redox reactions; COMSOL simulation of interfacial electric fields; and HRMS characterization of nitrogen disproportionation products (PDF)

AUTHOR INFORMATION

Corresponding Authors

Jianing Wang − *State Key Laboratory of Environmental and Biological Analysis, Department of Chemistry, Hong Kong Baptist University, Hong Kong, SAR 999077, P. R. China; School of Marine Science and Engineering, Hainan University, Haikou, Hainan 570228, P. R. China;*

https://doi.org/10.1021/acs.analchem.5c06042
Anal. Chem. 2026, 98, 850−859

orcid.org/0000-0002-9294-2809;
Email: justin.wang.4in1@gmail.com
Zhenwei Wei − *College of Chemistry and Molecular Sciences, Wuhan University, Wuhan, Hubei 430072, P. R. China;* orcid.org/0000-0001-7016-7787; Email: weizw2021@whu.edu.cn

Authors

Xiangyu Wang − *College of Chemistry and Molecular Sciences, Wuhan University, Wuhan, Hubei 430072, P. R. China; School of Public Health, Wuhan University, Wuhan, Hubei 430072, P. R. China;* orcid.org/0009-0007-5471-8594
Jin Han − *College of Chemistry and Molecular Sciences, Wuhan University, Wuhan, Hubei 430072, P. R. China*
Xin Diao − *College of Chemistry and Molecular Sciences, Wuhan University, Wuhan, Hubei 430072, P. R. China*
Xiaofei Wang − *College of Chemistry and Molecular Sciences, Wuhan University, Wuhan, Hubei 430072, P. R. China*
Chen Zeng − *College of Chemistry and Molecular Sciences, Wuhan University, Wuhan, Hubei 430072, P. R. China*
Yongyi Li − *College of Chemistry and Molecular Sciences, Wuhan University, Wuhan, Hubei 430072, P. R. China*
Zongwei Cai − *State Key Laboratory of Environmental and Biological Analysis, Department of Chemistry, Hong Kong Baptist University, Hong Kong, SAR 999077, P. R. China; Eastern Institute of Technology, Ningbo, Zhejiang 315200, P. R. China;* orcid.org/0000-0002-8724-7684

Complete contact information is available at: https://pubs.acs.org/10.1021/acs.analchem.5c06042

Author Contributions

#X.W. and J.H. contributed equally to this work.

Notes

The authors declare no competing financial interest.

■ ACKNOWLEDGMENTS

Z.W. acknowledges the National Key R&D Program of China (No. 2023YFF0723100), the National Natural Science Foundation of China (No. 22374110, No. 22574127), and the Fundamental Research Funds for the Central Universities. J.W. and Z.C. acknowledge the National Natural Science Foundation of China (No. 32450190) and the General Research Fund (No. 12302122) from the Research Grants Council of the Hong Kong Special Administrative Region. X.W. acknowledges support from the National Natural Science Foundation of China (No. 22504100), the China Postdoctoral Science Foundation (No. 2024M762465), and the open subsidies for large-scale instruments and equipment at Wuhan University.

■ REFERENCES

(1) Yan, X.; Bain, R. M.; Cooks, R. G. Organic reactions in microdroplets: Reaction acceleration revealed by mass spectrometry. *Angew. Chem., Int. Ed.* **2016**, *55* (42), 12960−12972.
(2) Wei, Z.; Li, Y.; Cooks, R. G.; Yan, X. Accelerated Reaction Kinetics in Microdroplets: Overview and Recent Developments. *Annu. Rev. Phys. Chem.* **2020**, *71* (1), 31−51.
(3) Girod, M.; Moyano, E.; Campbell, D. I.; Cooks, R. G. Accelerated bimolecular reactions in microdroplets studied by desorption electrospray ionization mass spectrometry. *Chem. Sci.* **2011**, *2* (3), 501−510.
(4) Qiu, L.; Morato, N. M.; Huang, K.-H.; Cooks, R. G. Spontaneous Water Radical Cation Oxidation at Double Bonds in Microdroplets. *Front. Chem.* **2022**, *10*, 903774.
(5) Jin, S.; Chen, H.; Yuan, X.; Xing, D.; Wang, R.; Zhao, L.; Zhang, D.; Gong, C.; Zhu, C.; Gao, X.; Chen, Y.; Zhang, X. The Spontaneous Electron-Mediated Redox Processes on Sprayed Water Microdroplets. *JACS Au* **2023**, *3* (6), 1563−1571.
(6) Spoorthi, B.; Debnath, K.; Basuri, P.; Nagar, A.; Waghmare, U. V.; Pradeep, T. Spontaneous weathering of natural minerals in charged water microdroplets forms nanomaterials. *Science* **2024**, *384* (6699), 1012−1017.
(7) Xia, D.; Zhang, H.; Ju, Y.; Xie, H.-b.; Su, L.; Ma, F.; Jiang, J.; Chen, J.; Francisco, J. S. Spontaneous Degradation of the "Forever Chemicals" Perfluoroalkyl and Polyfluoroalkyl Substances (PFASs) on Water Droplet Surfaces. *J. Am. Chem. Soc.* **2024**, *146* (16), 11266−11271.
(8) Meng, Y.; Gnanamani, E.; Zare, R. N. Catalyst-Free Decarboxylative Amination of Carboxylic Acids in Water Microdroplets. *J. Am. Chem. Soc.* **2023**, *145* (1), 32−36.
(9) Gnanamani, E.; Yan, X.; Zare, R. N. Chemoselective N-alkylation of indoles in aqueous microdroplets. *Angew. Chem., Int. Ed.* **2020**, *59* (8), 3069−3072.
(10) Jiang, Q.; Xia, D.; Li, X.; Zhang, H.; Yin, R.; Xie, H.; Xie, H. b.; Jiang, J.; Chen, J.; Francisco, J. S. Rapid N2O formation from N2 on water droplet surfaces. *Angew. Chem., Int. Ed.* **2025**, *137* (9), No. e202421002.
(11) Zhou, Z.; Yan, X.; Lai, Y.-H.; Zare, R. N. Fluorescence Polarization Anisotropy in Microdroplets. *J. Phys. Chem. Lett.* **2018**, *9* (11), 2928−2932.
(12) Mehrgardi, M. A.; Mofidfar, M.; Zare, R. N. Sprayed Water Microdroplets Are Able to Generate Hydrogen Peroxide Spontaneously. *J. Am. Chem. Soc.* **2022**, *144* (17), 7606−7609.
(13) Lee, J. K.; Walker, K. L.; Han, H. S.; Kang, J.; Prinz, F. B.; Waymouth, R. M.; Nam, H. G.; Zare, R. N. Spontaneous generation of hydrogen peroxide from aqueous microdroplets. *Proc. Natl. Acad. Sci. U.S.A.* **2019**, *116* (39), 19294−19298.
(14) Gao, D.; Jin, F.; Lee, J. K.; Zare, R. N. Aqueous microdroplets containing only ketones or aldehydes undergo Dakin and Baeyer−Villiger reactions. *Chem. Sci.* **2019**, *10* (48), 10974−10978.
(15) Song, X.; Basheer, C.; Zare, R. N. Water Microdroplets-Initiated Methane Oxidation. *J. Am. Chem. Soc.* **2023**, *145* (50), 27198−27204.
(16) Zhang, D.; Yuan, X.; Gong, C.; Zhang, X. High Electric Field on Water Microdroplets Catalyzes Spontaneous and Ultrafast Oxidative C−H/N−H Cross-Coupling. *J. Am. Chem. Soc.* **2022**, *144* (35), 16184−16190.
(17) Grooms, A. J.; Huttner, R. T.; Stockwell, M.; Tadese, L.; Marcelo, I. M.; Kass, A.; Badu-Tawiah, A. K. Programmable C−N Bond Formation through Radical-Mediated Chemistry in Plasma-Microdroplet Fusion. *Angew. Chem., Int. Ed.* **2025**, *137* (4), No. e202413122.
(18) Lee, J. K.; Samanta, D.; Nam, H. G.; Zare, R. N. Micrometer-Sized Water Droplets Induce Spontaneous Reduction. *J. Am. Chem. Soc.* **2019**, *141* (27), 10585−10589.
(19) Yuan, X.; Zhang, D.; Liang, C.; Zhang, X. Spontaneous Reduction of Transition Metal Ions by One Electron in Water Microdroplets and the Atmospheric Implications. *J. Am. Chem. Soc.* **2023**, *145* (5), 2800−2805.
(20) Lee, J. K.; Samanta, D.; Nam, H. G.; Zare, R. N. Spontaneous formation of gold nanostructures in aqueous microdroplets. *Nat. Commun.* **2018**, *9* (1), 1562.
(21) Zhao, L.; Song, X.; Gong, C.; Zhang, D.; Wang, R.; Zare, R. N.; Zhang, X. Sprayed water microdroplets containing dissolved pyridine spontaneously generate pyridyl anions. *Proc. Natl. Acad. Sci. U.S.A.* **2022**, *119* (12), No. e2200991119.
(22) Chen, H.; Wang, R.; Xu, J.; Yuan, X.; Zhang, D.; Zhu, Z.; Marshall, M.; Bowen, K.; Zhang, X. Spontaneous Reduction by One Electron on Water Microdroplets Facilitates Direct Carboxylation with CO2. *J. Am. Chem. Soc.* **2023**, *145* (4), 2647−2652.

(23) Gong, C.; Li, D.; Li, X.; Zhang, D.; Xing, D.; Zhao, L.; Yuan, X.; Zhang, X. Spontaneous Reduction-Induced Degradation of Viologen Compounds in Water Microdroplets and Its Inhibition by Host−Guest Complexation. *J. Am. Chem. Soc.* **2022**, *144* (8), 3510−3516.
(24) Xiong, H.; Lee, J. K.; Zare, R. N.; Min, W. Strong Electric Field Observed at the Interface of Aqueous Microdroplets. *J. Phys. Chem. Lett.* **2020**, *11* (17), 7423−7428.
(25) Chamberlayne, C. F.; Zare, R. N. Simple model for the electric field and spatial distribution of ions in a microdroplet. *J. Chem. Phys.* **2020**, *152* (18), 184702.
(26) Chamberlayne, C. F.; Zare, R. N. Microdroplets can act as electrochemical cells. *J. Chem. Phys.* **2022**, *156* (5), 054705.
(27) Lhee, S.; Lee, J. K.; Kang, J.; Kato, S.; Kim, S.; Zare, R. N.; Nam, H. G. Spatial localization of charged molecules by salt ions in oil-confined water microdroplets. *Sci. Adv.* **2020**, *6* (41), No. eaba0181.
(28) Hao, H.; Leven, I.; Head-Gordon, T. Can electric fields drive chemistry for an aqueous microdroplet? *Nat. Commun.* **2022**, *13* (1), 280.
(29) Gong, K.; Ao, J.; Li, K.; Liu, L.; Liu, Y.; Xu, G.; Wang, T.; Cheng, H.; Wang, Z.; Zhang, X.; Wei, H.; George, C.; Mellouki, A.; Herrmann, H.; Wang, L.; Chen, J.; Ji, M.; Zhang, L.; Francisco, J. S. Imaging of pH distribution inside individual microdroplet by stimulated Raman microscopy. *Proc. Natl. Acad. Sci. U.S.A.* **2023**, *120* (20), No. e2219588120.
(30) Heindel, J. P.; LaCour, R. A.; Head-Gordon, T. The role of charge in microdroplet redox chemistry. *Nat. Commun.* **2024**, *15* (1), 3670.
(31) Gan, T.; Yang, Z.; Li, S.; Qian, H.; Li, Z.; Liu, J.; Peng, P.; Bai, J.; Liu, H.; Wang, Z.; et al. Unveiling Janus Chemical Processes in Contact-Electro-Chemistry through Oxygen Reduction Reactions. *J. Am. Chem. Soc.* **2025**, *147* (29), 25407−25416.
(32) Li, X.; Nong, X.; Zhu, C.; Gao, X.; Chen, H.; Yuan, X.; Xing, D.; Liu, L.; Liang, C.; Zang, D.; et al. Atomization by Acoustic Levitation Facilitates Contactless Microdroplet Reactions. *J. Am. Chem. Soc.* **2024**, *146* (43), 29267−29271.
(33) Lin, S. Q.; Cao, L. N. Y.; Tang, Z.; Wang, Z. L. Size-dependent charge transfer between water microdroplets. *Proc. Natl. Acad. Sci. U.S.A.* **2023**, *120* (31), No. e2307977120.
(34) Chen, H.; Li, X.; Li, B.; Chen, Y.; Ouyang, H.; Li, Y.; Zhang, X. Microdroplet chemistry with unactivated droplets. *J. Am. Chem. Soc.* **2025**, *147* (13), 11399−11406.
(35) De Hoffmann, E.; Stroobant, V. *Mass Spectrometry: Principles and Applications*; John Wiley & Sons, 2007.
(36) Gross, J. H. *Mass Spectrometry: A Textbook*; Springer Science & Business Media, 2006.
(37) Zilch, L. W.; Maze, J. T.; Smith, J. W.; Ewing, G. E.; Jarrold, M. F. Charge separation in the aerodynamic breakup of micrometer-sized water droplets. *J. Phys. Chem. A* **2008**, *112* (51), 13352−13363.
(38) Zilch, L. W.; Maze, J. T.; Smith, J. W.; Jarrold, M. F. Freezing, fragmentation, and charge separation in sonic sprayed water droplets. *Int. J. Mass spectrom.* **2009**, *283* (1−3), 191−199.
(39) Yergey, A. L.; Edmonds, C. G.; Lewis, I. A.; Vestal, M. L. *Liquid chromatography/mass Spectrometry: Techniques and Applications*; Springer Science & Business Media, 2013.
(40) Twomey, S. The electrification of individual cloud droplets. *Tellus* **1956**, *8* (4), 445−452.
(41) Zhang, L.; Gu, Z.; Yu, C.; Zhang, Y.; Cheng, Y. Surface charges on aerosol particles−accelerating particle growth rate and atmospheric pollution. *Indoor Built Environ* **2016**, *25* (3), 437−440.
(42) Harrison, R. G.; Ambaum, M. H. Enhancement of cloud formation by droplet charging. *Proc. R. Soc. A* **2008**, *464* (2098), 2561−2573.
(43) Kulkarni, P.; Baron, P. A.; Willeke, K. *Aerosol Measurement: Principles, Techniques, and Applications*; John Wiley & Sons, 2011.
(44) Li, A.; Hollerbach, A.; Luo, Q.; Cooks, R. G. On-demand ambient ionization of picoliter samples using charge pulses. *Angew. Chem., Int. Ed.* **2015**, *54* (23), 6893−6895.
(45) Wei, Z.; Xiong, X.; Guo, C.; Si, X.; Zhao, Y.; He, M.; Yang, C.; Xu, W.; Tang, F.; Fang, X.; et al. Pulsed direct current electrospray: enabling systematic analysis of small volume sample by boosting sample economy. *Anal. Chem.* **2015**, *87* (22), 11242−11248.
(46) Van Berkel, G. J.; Zhou, F. Characterization of an electrospray ion source as a controlled-current electrolytic cell. *Anal. Chem.* **1995**, *67* (17), 2916−2923.
(47) Van Berkel, G. J.; Giles, G. E.; Bullock; Gray, L. J. Computational simulation of redox reactions within a metal electrospray emitter. *Anal. Chem.* **1999**, *71* (23), 5288−5296.
(48) Cech, N. B.; Enke, C. G. Practical implications of some recent studies in electrospray ionization fundamentals. *Mass Spectrom. Rev.* **2001**, *20* (6), 362−387.
(49) Salin, K.; Auer, S. K.; Villasevil, E. M.; Anderson, G. J.; Cairns, A. G.; Mullen, W.; Hartley, R. C.; Metcalfe, N. B. Using the MitoB method to assess levels of reactive oxygen species in ecological studies of oxidative stress. *Sci. Rep.* **2017**, *7* (1), 41228.
(50) Zielonka, J.; Sikora, A.; Hardy, M.; Joseph, J.; Dranka, B. P.; Kalyanaraman, B. Boronate probes as diagnostic tools for real time monitoring of peroxynitrite and hydroperoxides. *Chem. Res. Toxicol.* **2012**, *25* (9), 1793−1799.
(51) Liu, Q.; Ge, W.; Martínez-Jarquín, S.; He, Y.; Wu, R.; Stoffel, M.; Zenobi, R. Mass spectrometry reveals high levels of hydrogen peroxide in pancreatic cancer cells. *Angew. Chem., Int. Ed.* **2023**, *62* (19), No. e202213703.
(52) Li, K.; Guo, Y.; Nizkorodov, S. A.; Rudich, Y.; Angelaki, M.; Wang, X.; An, T.; Perrier, S.; George, C. Spontaneous dark formation of OH radicals at the interface of aqueous atmospheric droplets. *Proc. Natl. Acad. Sci. U.S.A.* **2023**, *120* (15), No. e2220228120.
(53) Qiu, L.; Cooks, R. G. Simultaneous and spontaneous oxidation and reduction in microdroplets by the water radical cation/anion pair. *Angew. Chem., Int. Ed.* **2022**, *134* (41), No. e202210765.
(54) Ben-Amotz, D. Electric buzz in a glass of pure water. *Science* **2022**, *376* (6595), 800−801.
(55) Kathmann, S. M.; Kuo, I.-F. W.; Mundy, C. J. Electronic effects on the surface potential at the vapor−liquid interface of water. *J. Am. Chem. Soc.* **2008**, *130* (49), 16556−16561.
(56) Shi, L.; LaCour, R. A.; Qian, N.; Heindel, J. P.; Lang, X.; Zhao, R.; Head-Gordon, T.; Min, W. Water structure and electric fields at the interface of oil droplets. *Nature* **2025**, *640*, 87−93.
(57) Liu, X.; Hu, F.; Ding, W.; Tian, R.; Li, R.; Li, H. A how-to approach for estimation of surface/Stern potentials considering ionic size and polarization. *Analyst* **2015**, *140* (21), 7217−7224.
(58) Wang, P.; Zhang, J.; Xu, F.; Wang, J.; Li, J.; Shen, Y.; Li, C.; Cui, X.; Li, S. Improving electric field strength of interfacial electric double layer and cycle stability of Li-ion battery via LiCl additive. *Electrochim. Acta* **2022**, *429*, 141060.
(59) Bard, A. J.; Faulkner, L. R.; White, H. S. *Electrochemical Methods: Fundamentals and Applications*; John Wiley & Sons, 2022.
(60) Hsiao, Y.; Chou, T.-H.; Patra, A.; Wen, Y.-C. Momentum-dependent sum-frequency vibrational spectroscopy of bonded interface layer at charged water interfaces. *Sci. Adv.* **2023**, *9* (15), No. eadg2823.
(61) García Rey, N.; Weißenborn, E.; Schulze-Zachau, F.; Gochev, G.; Braunschweig, B. r. Quantifying double-layer potentials at liquid−gas interfaces from vibrational sum-frequency generation. *J. Phys. Chem. C* **2019**, *123* (2), 1279−1286.
(62) Krem, S.; Lee, M.; Sam, S.; Sung, W.; Kim, D. Structure of electric double layer under cationic Langmuir monolayer: Charge condensation effect. *J. Phys. Chem. Lett.* **2021**, *12* (13), 3417−3423.
(63) Kumar, M.; Francisco, J. S. Ion pair particles at the air−water interface. *Proc. Natl. Acad. Sci. U.S.A.* **2017**, *114* (47), 12401−12406.
(64) Zhang, X.; Su, R.; Li, J.; Huang, L.; Yang, W.; Chingin, K.; Balabin, R.; Wang, J.; Zhang, X.; Zhu, W.; et al. Efficient catalyst-free N2 fixation by water radical cations under ambient conditions. *Nat. Commun.* **2024**, *15* (1), 1535.
(65) Greco, A.; Imoto, S.; Backus, E. H.; Nagata, Y.; Hunger, J.; Bonn, M. Ultrafast aqueous electric double layer dynamics. *Science* **2025**, *388* (6745), 405−410.

(66) Lowke, J.; D'Alessandro, F. Onset corona fields and electrical breakdown criteria. *J. Phys. D: Appl. Phys.* **2003**, *36* (21), 2673.
(67) Krajcar Bronić, I.; Grosswendt, B. Townsend ionization coefficients of some argon-based mixtures in strong nonuniform electric fields. *J. Appl. Phys.* **2000**, *88* (11), 6192−6200.
(68) Xia, Y.; Xu, J.; Li, J.; Chen, B.; Dai, Y.; Zare, R. N. Visualization of the charging of water droplets sprayed into air. *J. Phys. Chem. A* **2024**, *128* (28), 5684−5690.
(69) Bose, S.; Mofidfar, M.; Zare, R. N. Direct Conversion of N2 and Air to Nitric Acid in Gas−Water Microbubbles. *J. Am. Chem. Soc.* **2024**, *146* (40), 27964−27971.
(70) Anglada, J. M.; Martins-Costa, M. T.; Francisco, J. S.; Ruiz-López, M. F. Triplet state radical chemistry: Significance of the reaction of 3SO2 with HCOOH and HNO3. *J. Am. Chem. Soc.* **2024**, *146* (20), 14297−14306.
(71) Wang, Y.; Luo, J.; Fang, Y.-G.; Nan, Z.-A.; Cui, X.; Chen, T.; Zeng, X.; Wang, X.; Song, X.; Zhao, J.; et al. Catalyst-Free Nitrogen Fixation by Microdroplets through a Radical-Mediated Disproportionation Mechanism under Ambient Conditions. *J. Am. Chem. Soc.* **2025**, *147* (3), 2756−2765.
(72) Eatoo, M. A.; Wehbe, N.; Kharbatia, N.; Guo, X.; Mishra, H. Why do some metal ions spontaneously form nanoparticles in water microdroplets? Disentangling the contributions of the air−water interface and bulk redox chemistry. *Chem. Sci.* **2025**, *16* (3), 1115−1125.
(73) Majumder, T.; Eremin, D. B.; Delibas, B.; Sarkar, A.; Fokin, V.; Dawlaty, J. M. Calibrating the Oxidative Capacity of Microdroplets. *Angew. Chem., Int. Ed.* **2024**, *64* (2), No. e202414746.

https://doi.org/10.1021/acs.analchem.5c06042
Anal. Chem. 2026, 98, 850−859